Composition of the Secondary Particles Produced in Nuclear Interactions at $\sim 10^{12}$ eV*†

C. O. KIM
The Enrico Fermi Institute for Nuclear Studies
and
The Department of Physics, The University of Chicago, Chicago, Illinois
(Received 13 March 1964; revised manuscript received 15 June 1964)

Twenty-two proton, neutron, and alpha jets ($N_h \leq 3$, 2×10^{11} eV$<E<1.5\times10^{13}$ eV), found in a 22-liter emulsion stack flown for 13 h at an altitude of 116 000 feet, have been analyzed to identify the nature of the particles emitted in the extreme backward c.m. cone. Among 82 tracks analyzed, out of 149 tracks traced (total length of the secondaries traced was 20.4 m and 74 interactions were found), 53 secondaries were attributed to pions, 18 to kaons, 10 to protons, and one to a hyperon. The relative composition of the 82 secondaries has a dependence on the c.m. emission angle $\bar{\theta}$. For $\bar{\theta}\geq175°$, there were 7 π, 9 K, 10 p, and 1 Y; for $\bar{\theta}<175°$, there were 46 π, 9 K, and no baryons. A similar distinction existed for the average c.m. momenta $<\bar{p}>$ and the average transverse momenta $<p_t>$ in the extreme backward c.m. emission angle; $<\bar{p}>$ becomes large and $<p_t>$ becomes small. The baryons carried the average fraction 0.5 ± 0.2 of the total available energy in the c.m. system. Concerning the K/π ratio, p_t distribution, and $<\bar{p}>$ at $\theta<175°$, the hydrodynamical theory with a critical temperature $kT_c\cong m_\pi c^2$ predicts the correct behavior. In this region, the c.m. momentum distribution of pions fits the form $dN\propto\bar{p}^n\,d\bar{p}$ with $n=-0.8\pm0.4$. But for the extreme backward c.m. emission angle region, $\bar{\theta}\geq175°$, the smallness of $<p_t>$ and concentration of kaons and baryons favor an interpretation in terms of the Heisenberg theory.

I. INTRODUCTION

IN the very-high-energy nuclear interactions, a large fraction of the created particles are narrowly collimated in the direction of the primary incoming particles as a consequence of the great velocity of the c.m. system of the incident and target particles. These events, which are produced by high-energy cosmic rays and recorded mostly by means of big emulsion stacks flown by balloons at the top of the atmosphere, are known as "jets." There are excellent review articles available on the subject.[1,2] It is well established that the created particles (secondaries) are composed mostly of pions. The exact relative frequencies of occurrence of pions, kaons, nucleons, and hyperons are, however, not well known. At accelerator energies up to $\sim$30 GeV, this problem has been investigated fairly well,[3,4] and the question is open as to whether such frequencies remain constant at higher energies.

Two *indirect* methods have been used to investigate this problem.[1,2] A first approach consists in the measurement of the frequency of electron pairs versus that of charged secondaries in the core of jets. Since electron pairs are assumed to arise from the materialization of decay gamma rays of neutral pions, the frequency of these electron pairs gives an estimate of the production rate of neutral pions. The number of created charged pions is then inferred to be equal to twice the number of neutral pions, since charge independence is expected to hold in the production process, provided the pions are produced directly. Then the number of charged secondaries minus the number of charged pions in a given solid angle will give the portion of nonpionic charged secondaries. A second estimate is obtained from the observation of the frequency of secondary nuclear interactions produced by neutral particles, which are definitely nonpionic in origin. Both methods give an estimate of about 20% for the frequency of nonpionic secondaries at energies above 10^{12} eV.

The *direct* approach to this problem is concerned with the identification of the secondaries emitted backward in the c.m. system of the two colliding nucleons, with respect to the direction of the incident particle. In fact, the masses of such secondaries can be often established by measurements of grain density, scattering, and range

* Research supported by the National Science Foundation and the U. S. Office of Naval Research.

† This paper is based on a thesis submitted to the Department of Physics, the University of Chicago, in partial fulfillment of the requirements for the Ph.D. degree (August, 1963). Preliminary reports of this work were given in Bull. Am. Phys. Soc. 8, 293 (1963) and in the *Proceedings of the International Conference on Cosmic Rays of Jaipur, India, December 1963* (Tata Institute of Fundamental Research, Bombay, India, 1964), Vol. V.

[1] M. Koshiba, Brookhaven National Laboratory Report No. BNL 772 (T-290), 1961, p. 18 (unpublished); *Proceedings of International Conference on Cosmic Rays at Jaipur, India, 1963* (Tata Institute of Fundamental Research, Bombay, India, 1964), Vol. V.

[2] D. H. Perkins, *Progress in Elementary Particle and Cosmic Ray Physics* (North-Holland Publishing Co., Amsterdam, 1960), Vol. V, p. 257; in *International Conference on Theoretical Aspects of Very High-Energy Phenomena, 1961* (CERN Scientific Information Service, Geneva, 1961), p. 97.

[3] V. T. Cocconi, T. Tazzini, G. Fidecaro, M. Legros, *et al.*, Phys. Rev. Letters 5, 19 (1960); G. Cocconi, *Proceedings of the 1960 Annual International Conference on High Energy Physics at Rochester*, edited by E. C. G. Sandarshan, J. H. Tinlot, and A. C. Melissions, (Interscience Publishers, Inc., New York, 1960), p. 800; L. Gilly, B. Leontic, A. Lundby, R. Mennier, J. P. Stroot, and M. Szeptycka, *ibid.*, p. 837; W. F. Baker, R. L. Cool, E. W. Jenkins, T. F. Kycia, S. J. Lindenbaum *et al.*, Phys. Rev. Letters 7, 101 (1961); V. L. Fitch, S. L. Meyer, and P. A. Piroué, Phys. Rev. 126, 1849 (1962); A. Schwarzschild and C. Zupančič, *ibid.* 129, 854 (1963).

[4] H. Filthuth, in *Proceedings of the Aix-en-Provence International Conference on Elementary Particles, 1961* (Centre d'Etudes Nucléaires de Saclay; Seine et Oise, 1961), Vol. 1, p. 93.

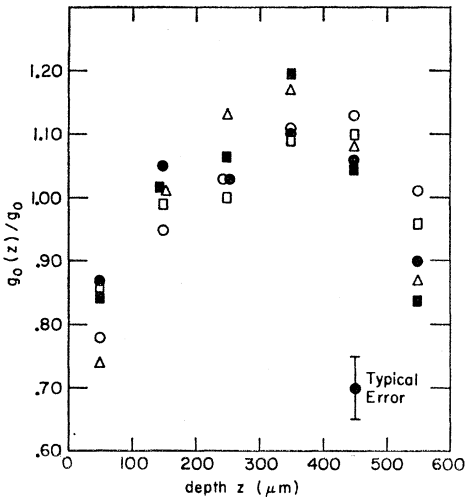

FIG. 1. Typical normalized grain density as a function of emulsion depth. Each symbol refers to a specific plate.

when they emerge in the laboratory system with energies $\lesssim 10$ GeV.[5,6] On the other hand, the forward-emitted secondaries are too energetic in the laboratory system for identification by conventional methods. However, several plausible models of a single nucleon-nucleon collision suggest that the secondaries in the backward and forward cones must possess, on the average, over-all symmetry with respect to the center of mass, as to both composition and angular distribution. Brisbout *et al.*[7] further attempted to estimate the nonpionic portion of secondaries from an analysis of the tertiary products emerging from the interactions of the backward-cone secondaries. In their study the tracks of secondaries were followed for 17 m and 51 interactions were observed, 32 of which were studied; one kaon and one hyperon were observed among the tertiary particles. One unstable secondary was also reported.

The present investigation follows the above authors' approach. The energy of the jets studied here is in the range of 2×10^{11} to 1.5×10^{13} eV. An attempt has been made to identify 149 secondaries belonging to the c.m. backward cone. The large volume of the stack employed here (22 liters) was used to full advantage. Not only multiple scattering and ionization measurements could be performed on very long tracks, but in several cases the variation of ionization along the path of the secondaries could be detected. In this way 82 of the secondaries studied could be identified.

Finally, several important features of high-energy nucleon-nucleon collisions are investigated here, such as the longitudinal and transverse momentum distributions of the secondaries in the c.m. system and the dependence of these quantities on emission angles and particle composition. This line of analysis follows the extensive investigations by the Chicago group led by the late Professor Marcel Schein.[8]

II. EXPERIMENTAL MATERIAL

1. Properties of the Emulsion Stack

A 22-liter stack of Ilford G-5 emulsion, consisting of 200 pellicles, each 60 cm$\times$30 cm$\times$600 microns, exposed over Texas at an altitude of 116 000 ft for 13 h, was used for the present experiment. Many investigations on various aspects of high-energy phenomena based on the material contained in this stack were previously reported.[9–16] Data referring to the flight curve, the construction of the stack and scanning procedures are contained particularly in Refs. 9 and 11.

Several details, pertinent to the present investigation, should, however, be mentioned here. The stack was processed in batches of 36 plates per day by the "dry" method of Bonetti *et al.*[17] Three months elapsed between exposure and development, while the new Ryerson processing plant was built.

The mean grain densities g_0 of high-energy electrons remain reasonably constant around $\langle g_0\rangle = 15.47$ grains per 100 microns for the group of plates No. 1–112, which were processed last. The fluctuation of grain density for the rest of the plates can be attributed to the setting-up of the routine in the new processing plant. The tracks of high-energy electrons were carefully selected from the electromagnetic showers and were estimated to have energies ≈ 100 MeV, or within about 2% of the relativistic plateau of grain density. The depth dependence of grain density $g_0(z)$ of the high-energy electrons on the depth z, measured from the glass surface of the emulsion, was constructed for several plates and was tested using the very high energy electron pairs in the cores of jets. Figure 1 shows the typical dependence of the grain density, $g_0(z)$, which is normalized by g_0 of the plate where $g_0 = \int g_0(z)dz/\int dz$. In spite of the large variation with the depth the mean

[5] R. R. Daniel, J. H. Davies, J. H. Mulvey, and D. H. Perkins, Phil. Mag. **43**, 753 (1952).
[6] B. Edwards, J. Losty, K. Pinkau, D. H. Perkins, and J. Reynolds, Phil. Mag. **3**, 237 (1958).
[7] F. Brisbout, C. Dahanayake, A. Engler, P. Fowler, and P. Jones, Nuovo Cimento **3**, 1400 (1956).
[8] M. Schein, R. G. Glasser, and D. M. Haskin, Nuovo Cimento **2**, 647 (1955); R. G. Glasser, D. M. Haskin, M. Schein, and J. J. Lord, Phys. Rev. **99**, 1555 (1955); E. Lohrmann, Nuovo Cimento **5**, 1074 (1957); M. W. Teucher, D. M. Haskin, and M. Schein, Phys. Rev. **111**, 1384 (1958); M. Schein, D. M. Haskin, E. Lohrmann, and M. W. Teucher, *ibid.* **116**, 1238 (1959).
[9] A. G. Barkow, B. Chamany, D. M. Haskin, P. L. Jain, E. Lohrmann *et al.*, Phys. Rev. **122**, 617 (1961).
[10] P. L. Jain, Phys. Rev. **122**, 1890 (1961); Nuovo Cimento **24**, 698 (1962).
[11] J. Kidd, Nuovo Cimento **27**, 57 (1963).
[12] M. Teucher, E. Lohrmann, D. M. Haskin, and M. Schein, Phys. Rev. Letters **2**, 313 (1959); Nuovo Cimento **17**, 986 (1960).
[13] P. L. Jain, Phys. Rev. **125**, 679 (1962).
[14] J. Gierula, D. M. Haskin, and E. Lohrmann, Phys. Rev. **122**, 626 (1961).
[15] E. Lohrmann, M. W. Teucher, and M. Schein, Phys. Rev. **122**, 672 (1961).
[16] E. Lohrmann, Phys. Rev. **122**, 1908 (1961).
[17] A. Bonetti, C. Dilworth, G. P. S. Occhialini, Bulletin of the University Bruxelles, No. 13 b, 1951 (unpublished).

grain density g_0 was consistently the same over different regions for each plate.

The one-millimeter LRL grid[18] was photographically printed on the glass side of the emulsion and these coordinate readings were used for the range measurements and for aid in tracing. The alignment of the grid from a plate to the next was well within $\frac{1}{2}$ mm. The grid system and the "landmarks" provided by local tracks enabled about 10 000 traversals of shower particles and tertiary particles between plates to be successfully traced with about 26 impossible cases, which resulted mostly from crossing the cut edges which became ragged after cutting.

The stack had two shortcomings: (i) No systematic measurements of thickness of the emulsion prior to development were made. (ii) The density of the emulsion during the flight is not known. Thus, all the plates in the stack were assumed to be exactly 600 microns before processing and of the standard density, 3.815 gm/cm³. The results of the present experiment, however, mostly based on measurements of multiple Coulomb scattering and ionization, are particularly insensitive to variation in such parameters, at least within the limits known for typical emulsion stacks.

2. Scanning

Each plate of this stack was scanned with 22× oil objectives and 12.5× oculars for groups of parallel and minimum ionizing tracks along scanning lines defining 15-cm×15-cm squares. From about 2000 groups of associated shower tracks that were found on the scanning lines, all showers having more than ten parallel tracks in one field of view were traced back to their origin.[11] The scanning criterion corresponds to a lower limit of about 100 GeV for the energy contained in the electron-photon component of the showers. A total of 120 nuclear interactions (78 p, 6n, 27α, and 9 heavies) were found. Among 84 p or n events, 57 events with dip angles less than 17° were analyzed and reported by Barkow *et al.*[9] Jain[10] reported the results of the analysis of 17 alpha jets with dip angles less than 20°.

3. Selection of Jets and of Tracks for Analysis

Among these nuclear interactions, 22 jets of proton, alpha, or neutral primaries, which satisfied the following criteria, were chosen for the present study:

(i) The primary had a track length of more than 2 mm per plate.

(ii) The potential length of the jet axis in the stack was larger than 20 cm.

(iii) The number of grey or heavy tracks, $N_h \leq 3$.

(iv) The estimated energy was greater than 10^{11} eV.

Condition (i) was imposed to ensure having the secondaries of favorable geometry, condition (ii) gives the secondaries more chances to interact in the detector, and condition (iii) selects either primaries' collision with hydrogen or with emulsion nuclei in which the effect of collisions with more than one nucleon is minimal. The relevant data for these events are listed in Table I. Indicated are the event number, the type of jet in accordance with the standard nomenclature (n_s corresponds to the number of secondaries with the normalized grain density $g^*<1.5$), the Castagnoli energy E_{Cast},[19] the energy carried by the charged secondaries defined as $E_{\text{ch}}=[\sum 0.4\ \text{GeV}/\sin\theta_i]$ by assuming the transverse momenta of the secondaries as 0.4 GeV/c and constant, the track length of primaries per plate, the spread of the distribution

$$\sigma=[\sum(\log_{10}\tan\theta_i-\langle\log_{10}\tan\theta_i\rangle)^2/(n_s-1)]^{1/2},$$

and the potential length of the jet axis in the stack. The emission angles θ_i refer to the centroid of the secondaries in the laboratory system. For most p and n events E_{Cast} and the particle multiplicities correspond to those given in Ref. 9. Only for event No. 63 a new energy estimate is given here. E_{ch} was calculated from the plot of $\log\tan\theta_i$ in Ref. 9. The seven alpha events were thoroughly reanalyzed. In all cases the emission angles of the backward-cone secondaries were carefully remeasured with respect to the direction of the incident primary.

Out of 501 shower particle tracks, the following were selected for measurement:

(i) All those belonging to $\frac{1}{8}$ of the charged secondaries in the extreme backward-cone. Such tracks were traced

TABLE I. Events studied.

Event No.	Type	E_{Cast} (TeV)	E_{ch}	σ	Dip (mm/p)	Potential Jet Axes (cm)
4	$2+17_p$	5.7	1.5	0.93	10.5	26
5	$2+5_p$	···	2.4	···	3.4	25
8	$0+41_\alpha$	3.3	4.2	0.84	218	25
9	$1+11_p$	0.60	0.22	0.76	2.9	45
12	$2+23_p$	9.9	3.7	1.03	3.2	32
13	$3+33_p$	2.5	2.2	0.76	4.6	40
23	$3+18_n$	5.4	0.93	0.71	2.4	44
28	$1+23_p$	3.0	3.4	0.98	11	31
41	$3+15_\alpha$	0.24	0.14	0.71	3.7	23
46	$3+41_\alpha$	0.33	0.78	0.67	2.8	31
47	$2+14_p$	12	1.8	0.92	293	41
49	$0+9_p$	1.7	0.43	0.81	14.8	30
59	$3+68_\alpha$	11	6.9	0.69	7.6	60
63	$2+20_p$	6.6	1.7	0.65	6.1	37
72	$1+27_p$	15	1.8	0.65	2.6	21
77	$3+43_\alpha$	0.67	1.3	0.74	47.3	22
109	$1+20_\alpha$	2.8	0.66	0.57	2.0	35
113	$0+4_\alpha$	···	8.2	···	7.2	24
116	$0+8_p$	0.23	0.58	0.49	78.2	44
117	$0+17_p$	1.5	0.70	0.67	4.3	32
118	$0+21_p$	15	2.2	0.69	476	28
120	$2+23_p$	6.2	3.2	1.11	2.1	34
	Average	5.2	2.2	0.77		

[18] By the courtesy of Professor W. H. Barkas. Berkeley mm-square grid.

[19] C. Castagnoli, G. Cortini, D. Moreno, C. Frazinetti, and A. Manfredini, Nuovo Cimento 10, 1539 (1953).

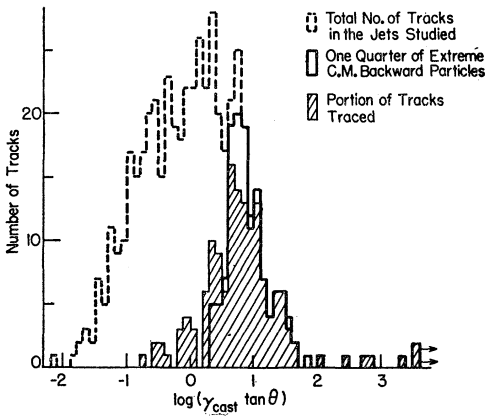

FIG. 2. Composite angular distribution of 501 secondaries (broken line); the bold line encloses $\frac{1}{4}$ of the total number of charged secondaries in the extreme backward cone; the shaded region indicates the tracks (149) actually traced.

to their ends in the stack, regardless of dip angles. Four grey tracks with the normalized grain density $1.5<g^*\leq 3.2$, later identified as protons, were also included in this analysis.

(ii) All tracks of length ≥ 5 mm per plate, not included in (i), to cover about $\frac{1}{4}$ of the charged secondaries in the extreme backward-cone. Such tracks were traced.

The composite angular distribution of the 22 jets is shown in Fig. 2. The solid line histogram refers to the tracks contained in $\frac{1}{4}$ of the charged secondaries in the backward-cone, while the shaded area represents the portion of secondaries which were actually traced. In addition, the grey and black prongs of all the primary interactions were also traced to their ends in the stack. When the secondaries being followed interacted, the numbers of black, grey, and shower particles in the secondary stars were carefully determined. Grey and black tertiary particles from all the secondary interactions were then in turn traced throughout the stack.

A total of 74 interactions was found in tracing 20.4 m of secondaries. (The corresponding interaction mean free path is 27.2 cm in place of the geometrical mean free path in emulsion of 28 cm.) Twenty-six tracks out of 149 were lost in tracing. Only one of the four grey secondaries included in the analysis came to rest among all the secondaries analyzed and was identified as a 130 MeV proton.

III. IDENTIFICATION OF JET SECONDARIES

Aside from the rare occurrence of decays in flight or strangeness-conserving interactions, the systematic identification of charged jet secondaries stems from the measurements of quantities depending on their electromagnetic interaction. Thus, the mass of a secondary was determined essentially with the following two standard methods, which were sometimes employed simultaneously:

(a) The parameter m_i in the function $g^*=f[(R_i/m_i)]$, where g^* is the grain density of a secondary normalized to that for shower electrons, $g^*=g/g_0$, and R_i the residual range, was determined by measuring the variation of the normalized grain density $\Delta g^*=g_2^*-g_1^*$ at a value of g_1^* over a distance, $\Delta R_i=R_{i2}-R_{i1}$. This was, of course, possible only if the thickness ΔR_i of emulsion traversed was large enough to moderate appreciably the energy of the secondary.

(b) The mass m_i in $p\beta=m_i\gamma\beta^2$ was determined by combining the value of the $p\beta$, obtained from measurement of multiple Coulomb scatterings with that of the normalized grain density g^*, which to a good approximation is a function only of the velocity β and not of the mass.

The function $g^*=f[(R_i/m_i)]$ could be established by measurements on known particles in the region of $\beta\lesssim 0.95$ (preminimum region), while $g^*=F(p\beta)$ beyond the minimum ionization (transminimum region) is essentially predicted on theoretical grounds; these functions were then used to attempt particle identification. The details of the grain density and scattering measurements are described in the Appendix.

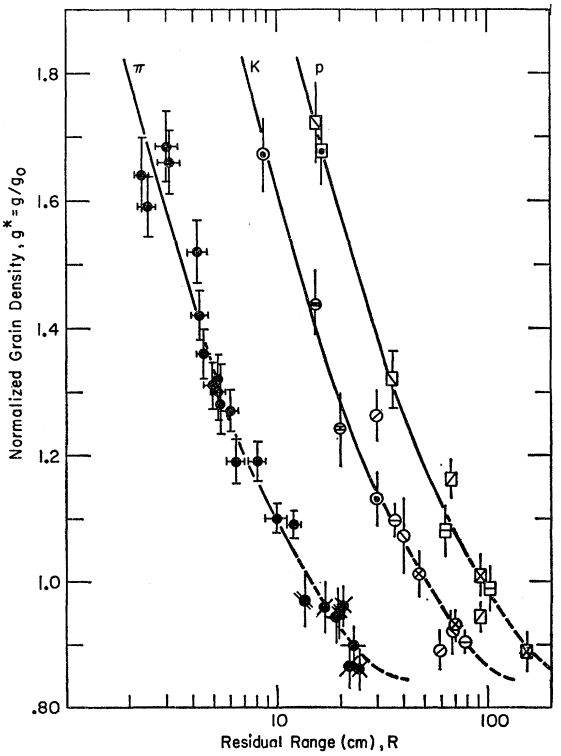

FIG. 3. Experimental variation of the normalized grain density according to residual range. π-mesons points at 2 cm $<R<12$ cm were taken on tracks of stopping π^+ mesons. The other points correspond to jet secondaries, where the two same symbols refer to the same secondary in a fit of g^* versus R.

1. Grain Density Calibration in the Pre-Minimum Region

The grain density in the region $0.62 \leq \beta \leq 0.83$ was established using tracks of stopping positive pions, identified by their characteristic π-μ-e decay. The pions were traced back from their decay points and counting was performed in the region of residual range from 2 to 12 cm. This calibration is shown in Fig. 3 where the solid curve is a best fit to the experimental points. The curves for kaons and protons were derived from the pion curve.

It was possible to extend the curve further down to the region of minimum ionization by observing the variations of g^* for jet secondaries, even if they did not stop or decay in the stack. This is shown in Fig. 3 where the observed variation in the normalized grain density, over an interval ΔR, is fitted to extrapolate the curves obtained up to $\beta \approx 0.95$. By this procedure some of the secondaries were also identified. The region thus calibrated is indicated by dashed curves in Fig. 3. The same symbol is used to represent points of the same secondary.

2. The Theoretical Grain Density in the Relativistic Region

The average energy loss per unit path by ionization of a singly charged particle of velocity β in units of the velocity of light c may be expressed by the modified Bethe-Bloch formula[20–22]

$$-\frac{dE}{dx}=\frac{2\pi n_e e^4}{mc^2\beta^2}\left(\ln\frac{2mc^2\beta^2\gamma^2 T}{\omega^2}-2\beta^2-\Delta\right), \qquad (1)$$

where

n_e = number of electrons per unit volume,
m = electron mass,
$\gamma=(1-\beta^2)^{-1/2}$,
ω = average ionization potential of atoms in the medium,
T = maximum energy transfer to an electron; for a heavy particle of rest mass m_i, it is given by

$$T=\frac{(\gamma^2-1)m_i c^2}{m_i/2m+m/2m_i+\gamma},$$

Δ = the correction for the density effect.

However, as stressed by many authors,[21,23–25] the "restricted" rate of energy loss I_r which is to be compared with grain density in emulsion, arises from absorption *only* in AgBr crystals *along the track*, and can be expressed as

$$I_r=\frac{2\pi n_e' e^4}{mc^2\beta^2}\left(\ln\frac{2mc^2\beta^2\gamma^2 T_0}{\omega'^2}-\beta^2-\Delta'\right), \qquad (2)$$

where T_0 is the maximum energy of delta rays which are contained in the dimension of a single grain. The dashed quantities refer here to AgBr. The correction Δ' for the density effect, which is very critical for the present purpose, is approximated by the analytical expressions given by Sternheimer[26,27]:

$$\Delta'=\ln\beta^2\gamma^2+C'+0.0235(4-x)^{4.03}, \quad \text{for } 0.30<x<4,$$
$$\Delta'=\ln\beta^2\gamma^2+C', \quad \text{for } x\geq 4, \qquad (3)$$

where

$$x=\log_{10}\beta\gamma;$$
$$C'=-\ln[\omega'^2/(h\nu_p')^2]-1;$$
$$\nu_p'=(n_e' e^2/\pi m)^{1/2}.$$

So I_r in Eq. (2) becomes

$$I_r=\frac{2\pi n_e' e^4}{mc^2\beta^2}\left[\ln\frac{2mc^2 T_0}{(h\nu_p')^2}-\beta^2+1-0.0235(4-x)^{4.03}\right], \quad \text{for } 0.30<x<4,$$

and the asymptotic plateau value $I_r(\beta=1)$ becomes

$$I_r(\beta=1)=\frac{2\pi n_e' e^4}{mc^2}\ln\frac{2mc^2 T_0}{(h\nu_p')^2}, \qquad (4)$$

where there is no longer a dependence on the ionization potential as such, but only on the electron density n_e' in the medium linearly and through the plasma frequency ν_p'. Then the theoretical expression $g^{**}=I_r/I_r(\beta=1)$, which is to be compared with the normalized grain density g^*, is given as

$$g^{**}=\frac{\ln[2mc^2 T_0/(h\nu_p')^2]-\beta^2+1-0.0235(4-x)^{4.03}}{\beta^2\ln[2mc^2 T_0/(h\nu_p')^2]}. \qquad (5)$$

This expression predicts that the grain density should increase again to an asymptotic plateau value after passing through a broad minimum around $\beta_{\min}=0.954$. The existence of such relativistic rise to a plateau was first detected by Pickup and Voyvodic[28] and subsequently confirmed by many observations.[5,6,29–32]

[20] B. Rossi, *High-Energy Particles* (Prentice-Hall, Inc., New York, 1952), p. 24.
[21] M. M. Shapiro, *Handbuch der Physik*, edited by S. Flügge (Springer-Verlag, Berlin, 1958), Vol. XLV, p. 342.
[22] C. F. Powell, P. H. Fowler, and D. H. Perkins, *The Study of Elementary Particles by the Photographic Method* (Pergamon Press, Inc., London, 1959).
[23] H. Messel and D. M. Ritson, Phil. Mag. **41**, 1129 (1950).
[24] M. Schönberg, Nuovo Cimento **8**, 159 (1951).
[25] L. Brown, Phys. Rev. **90**, 95 (1953).
[26] R. M. Sternheimer, Phys. Rev. **88**, 851 (1952); **89**, 1148 (L) (1953); **91**, 256 (1953); **93**, 1434 (E) (1954); **93**, 351 (1954).
[27] R. M. Sternheimer, Phys. Rev. **103**, 511 (1956). This paper takes into consideration of the determination of the mean excitation potential I by Caldwell [D. O. Caldwell, Phys. Rev. **100**, 291 (1955)] as $I=13\,Z$ in contrast to $I=9.4\,Z$ in Ref. 26.
[28] E. Pickup and L. Voyvodic, Phys. Rev. **80**, 89 (L) (1950).
[29] H. A. Morrish, Phil. Mag. **43**, 533 (1952).
[30] M. Shapiro and B. Stiller, Phys. Rev. **87**, 682 (L) (1952); **92**, 735 (1953).
[31] G. Alexander and R. H. W. Johnston, Nuovo Cimento **5**, 363 (1957).
[32] J. W. Patrick and W. H. Barkas, Nuovo Cimento Suppl. **23**, 1 (1962).

TABLE II. The ratio of the asymptotic plateau value to the minimum grain density.

Author	Ratio	Type of emulsion	Highest γ for calibration
Pickup *et al.*[a]	1.10	G-5	~20
Morrish[b]	1.05	G-5	~25
Daniel *et al.*[c]	1.10	G-5	~20
Shapiro *et al.*[d]	1.14±0.03	G-5	3400
	(1.16±0.03)		(300)
Alexander *et al.*[e]	1.133±0.008	G-5	~500
Edwards *et al.*[f]	1.08	(G-5?)	?
Patrick *et al.*[g]	1.18	K-5, G-5	1400
Present work	1.23±0.03	G-5	10^4

[a] Reference 28. [b] Reference 29. [c] Reference 5. [d] Reference 30. [e] Reference 31. [f] Reference 6. [g] Reference 32.

Shapiro and Stiller[30] made a detailed comparison of the rate of relativistic rise with theory, and obtained a very good fit to the curve which included the density effect function elaborated by Sternheimer.[26] The comparison of Eq. (5) with experiment depends critically on the knowledge of the mean ionization potential ω' for AgBr. The value for this quantity chosen here is $\omega'=574$ eV as given by Sternheimer.[27] For the electron density in AgBr the value $n_e'=0.83\times10^{24}$ electrons/cm^3 has been used,[21] but the knowledge of n_e' is not very critical for the present experiment, since Eq. (5) does not depend on n_e' any more except through the weak dependence on the plasma frequency. The parameter T_0 is usually determined by the ratio between minimum and plateau grain densities. As will be obtained in the next section, $g^{**}_{\min}=0.81$ for the present experiment, which determines a value $T_0=0.9$ keV.

3. The Experimental Relativistic Rise in Grain Density

The experimental ratio between the grain densities at minimum and plateau ionization, respectively, was determined in the following manner. First, the normalized grain density of a proton primary (8 TeV, $\gamma=8.5\times10^3$) was observed to be $g^*_{\text{plateau}}=1.028\pm0.024$, where the normalization is relative to the electron grain density at $\gamma\simeq200$. The grain density at minimum ionization was determined from several of the measured pion secondaries. This corresponds to $g^*_{\min}=0.84\pm0.01$. The observed relativistic increase is then $(23\pm3)\%$. This result is compared in Table II with similar ones in previous experiments.

The theoretical function Eq. (5) of the previous section, for the choice of the critical parameters already described and for the trans-minimum region only, is reproduced in Fig. 4, where it is normalized to fit the experimental g^*_{plateau}. The pre-minimum part of the curve in Fig. 4 corresponds to the best fit of the g^* versus R plot of Fig. 3. For this translation, use was made of the range-energy relation of Barkas.[33] As can be seen, the experimental points g^*-$p\beta$ follow quite satisfactorily the slow rise to the plateau predicted by Sternheimer[27] and in this sense agree very well with the observations of Shapiro and Stiller[30] and of Patrick and Barkas.[32]

The contribution from the Čerenkov radiation, which was estimated by Sternheimer[26] and Allen[34] to amount at most to about 2% of the total increase of ionization from the minimum to the plateau, was not included in Eq. (5) of the previous section. The upper limit of this effect may be set to less than about 5% from the present experiment. In fact, the experimental points of jet secondaries around $\gamma=20$ lie, on the average, at most a percent higher than the predicted g^* curve of Fig. 4. Then by assuming (i) that this discrepancy is solely due to the Čerenkov contribution, which is believed to saturate very early around $\gamma=20$ and (ii) that the estimated theoretical g^* is accurate to less than a percent in this region, the above estimate follows. Of course, it should be kept in mind that the scattering measurements might have given an underestimate of $p\beta$ because of spurious scatterings. If this were indeed the case, any difference between experimental points for g^* versus $p\beta$ and the theoretical g^* would disappear, thus, reducing even further the above upper limit on the Čerenkov contribution.

4. Identity Assignments

Out of the 149 secondaries traced, 13 secondaries were identified by method (a) alone, 4 secondaries by the combination of both methods (a) and (b), and 65 secondaries by method (b) alone. Method (b) was used only for those secondaries which had track lengths ≥6 mm per plate and did not interact within 5 mm from the parent jet. Altogether, the analyzed portion is 55% of the tracks that were traced; i.e., 82 secondaries out of 149. Figure 5 shows, by a shaded histogram, the angular distribution of the secondaries which were analyzed.

Method (a) was used on the basis of Fig. 3. If a variation in g^* along the path of a secondary was detected, a fit to each curve in Fig. 3 was attempted. The best fit to one of the curves for a given ΔR gave the identity of the secondary. The calibration of the g^*-$p\beta$ function of Fig. 4 provides the basis for identification by method (b). As can be seen, a large number of points cluster around the pion curve, while several fit the kaon curve better. Pions were distinguished from kaons and protons in the region where the curves intercept, by the absence of a variation in g^*. In any case, for each event the relative probability of it belonging to either identity was estimated and an assignment made. The identity assignment of the 82 secondaries (except 3 protons of $g^*>1.8$) by all methods is illustrated in Fig. 4 where

[33] W. H. Barkas, University of California Radiation Laboratory Report No. UCRL 3384, 1956 (unpublished); B. H. Willis and C. V. Stableford, University of California Radiation Report No. UCRL 2426 (rev.), 1956 (unpublished).

[34] J. R. Allen, Phys. Rev. 93, 353 (L) (1954).

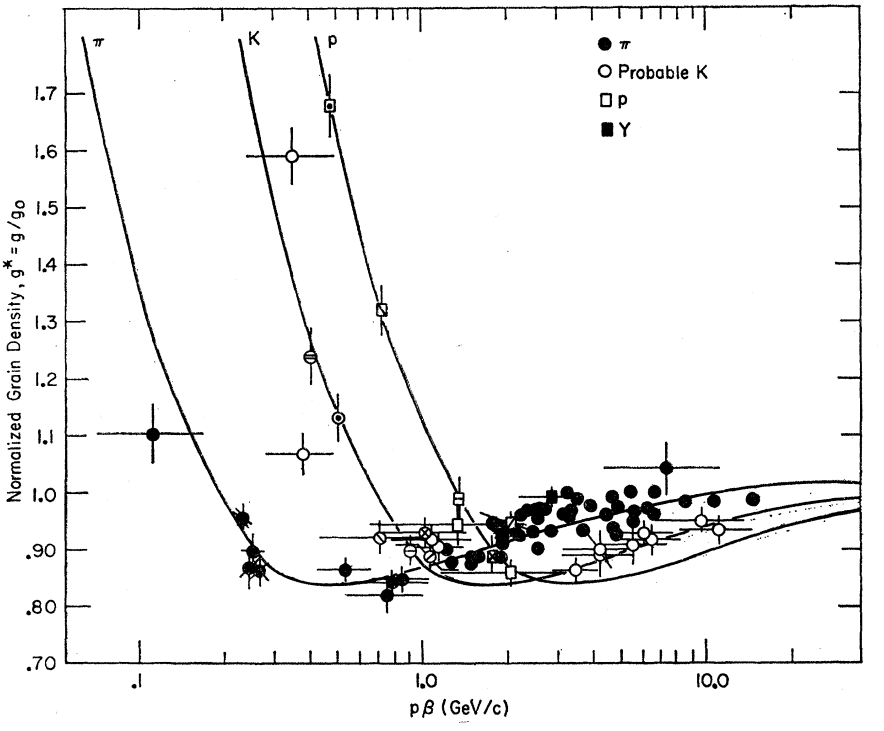

FIG. 4. Normalized grain density versus $p\beta$ for jet secondaries.

the black filled circles represent pions; the open circles, kaons; the open squares, protons; and a filled square, a hyperon, identified by its decay.[35] The secondaries, identified by method (a), are reported in Fig. 4 with the same symbols as in Fig. 3. It should be pointed out that three kaons and a proton were separated by the combination of both methods (a) and (b) from the pions in the transminimum region. One of the three kaons also produced a mesic hyperfragment.

IV. EXPERIMENTAL DATA

1. Composition of Secondaries

Among the 82 secondaries analyzed, 53 were attributed to pions, 18 to kaons, 10 to protons, and one to a hyperon; this corresponds to relative frequencies of production of $(65\pm9)\%$, $(22\pm5)\%$, $(12\pm4)\%$, and $(1\pm1)\%$, respectively, where the errors quoted are only statistical.[36]

The degree of discrimination between particles in the present set of data is shown by the two histograms in Fig. 6. The upper histogram of the two is the mass distribution of the 82 secondaries by folding the errors of g^* and $p\beta$, while the lower histogram shows the mass distribution of the identified secondaries when no errors in measurements of g^* and $p\beta$ were assumed. The mass values were calculated strictly with reference to the theoretical g^*-$p\beta$ curve of the pion for both cases. The similarity of shape and width in the distributions of the two histograms in Fig. 6 shows consistency in errors of measurements adopted.

It is realized that the separation is not very clear and the wrong identification is quite possible especially for those secondaries which lie in the intermediate regions between the peaks in the mass distribution in Fig. 6. An upper limit of contamination is estimated at about 10% of the so-called kaon and proton samples.

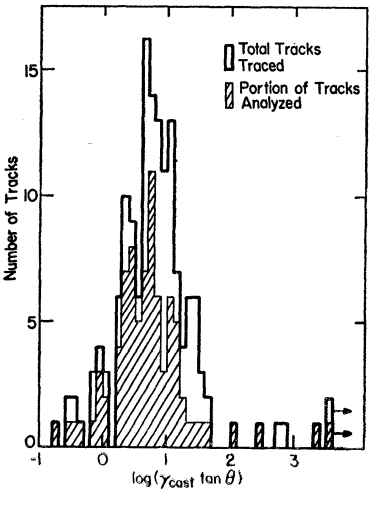

FIG. 5. Angular distribution of 149 tracks traced and 82 tracks analyzed.

[35] C. O. Kim, Enrico Fermi Institute of Nuclear Studies, Report 64–15 (unpublished).

[36] A table which shows the track number identified, $\tan\theta$, g_1^*, ΔR, g_2^*, $p\beta$, identity assigned, method used, and p_t is available upon request. Table VIII in Enrico Fermi Institute of Nuclear Studies, Report 64–12, which was the preprint of the present paper, contains several minor mistakes in $\tan\theta$ and accordingly p_t. The author is grateful to Professor R. W. Huggett for pointing them out from the computations on the original data.

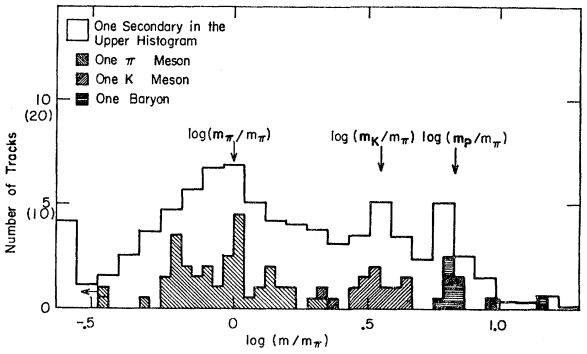

FIG. 6. Mass distribution according to the theoretical curve adopted. The upper histogram is a mass spectrum with experimental errors folded in.

With the help of E_{Cast} in Table I, the emission angle of each secondary was transformed into the c.m. system. The relative composition of the secondaries was found to be dependent on the c.m. emission angle $\bar{\theta}$ as shown in Table III.

TABLE III. Relative composition of the secondaries versus $\bar{\theta}$.

Range of c.m. Angle $\bar{\theta}$	Numbers Pion	Kaon	Proton	Hyperon
$\bar{\theta}\geq 175°$	7	9	10	1
$\bar{\theta}<175°$	46	9	...	...
Over-all	53	18	10	1

2. C.M. Momentum and Transverse Momentum Distribution

The results of the Lorentz transformation to the c.m. system are shown in Fig. 7 where the transverse momentum of the jet secondaries is plotted versus their longitudinal momentum. Figure 8 shows the momentum distributions of pion and kaon, where the shaded portion represents the secondaries with the c.m. emission angles $\geq 175°$. The average c.m. momenta of the pion and kaon are 2.1 and 8.1 GeV/c, respectively.

TABLE IV. Index of persistency.

Track No.	Identity	C.m. energy	$m_{p\gamma\text{Cast}}$	Index of persistency
4-15	p	15.1 GeV	52 GeV	0.29
8-1	p	29.3	39	0.75
8-28	p	8.8	39	0.23
9-1	p	6.9	17	0.41
12-1	p	73.9	68	1.09
13-1	p	8.5	35	0.24
41-2	p	7.8	10	0.78
59-2	p	17.3	72	0.24
72-G1	p	66.4	83	0.80
109-7	p	10.8	37	0.29
120-1	Y	38.4	53	0.72
	Average	28.3	(Excluding12-1)	0.48±0.15

The ratios of the c.m. energy of the 11 baryons (10 p, 1 Y) to half the available energy in the c.m. system corresponding to each primary, can be defined as an index of "persistency" for the baryons; Table IV lists the track number, c.m. energy, half the total available energy, and index of persistency of the 11 baryons. The average of this index thus obtained (excluding the track 12-1) is 0.5±0.2, which should not be influenced by the inaccuracy of the primary energy estimate to a good approximation. That track 12-1 has an index of persistency larger than 1 might have resulted from the wrong assignment of mass for the track.

The least square fit of the pion momentum distribution, for c.m. emission angle $\bar{\theta}<175°$, to the form $dN\propto\bar{p}^n d\bar{p}$ gives

$$n=-0.8\pm0.4, \tag{6}$$

and the best fit is drawn in Fig. 8.

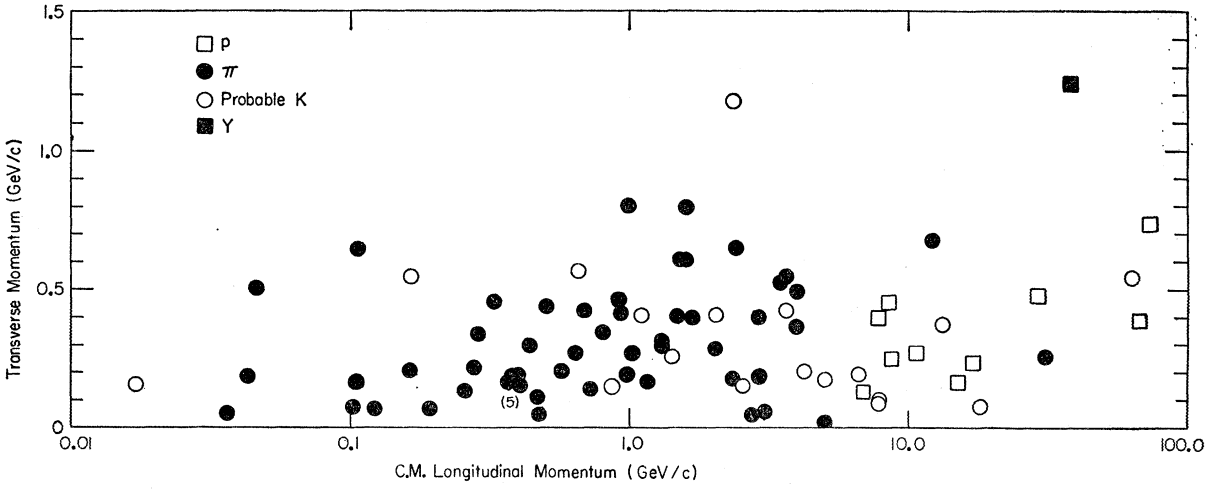

FIG. 7. C.m. longitudinal momentum versus transverse momentum.

TABLE V. Angular dependence of the average c.m. momentum and transverse momentum.

Range of c.m. angle $\bar{\theta}$	$\langle\bar{p}\rangle$ (GeV/c) π	K	p	$\langle p_t\rangle$ (GeV/c) π	K	p
$\bar{\theta}\geq 175°$	8.5	14.6	28	0.20±0.08[a]	0.21±0.07	0.35±0.11
$\bar{\theta}<175°$	1.1	1.5	···	0.32±0.05	0.45±0.15	···
Over-all	2.1	8.1	28	0.30	0.33	0.35

[a] Errors are only statistical.

The average transverse momentum of the secondaries has been given special attention,[37] since it has been known to be small and reasonably constant through a wide range of primary energies. Figure 9 shows the transverse momentum distributions of pions, kaons, and protons where the shaded portions are for the c.m. emission angle $\bar{\theta}\geq 175°$. The average transverse momenta of pions, kaons, and protons obtained from the present experiment are 0.30, 0.33, and 0.35 GeV/c, respectively. The hyperon observed above has an unusually large transverse momentum $p_t=1.3$ GeV/c.

The angular dependence of the c.m. average momenta $\langle\bar{p}\rangle$ and transverse momenta $\langle p_t\rangle$ of pions, kaons, and protons are listed in Table V. It should be emphasized again here that the secondaries analyzed in the present experiment were selected from the outer-cone particles in the laboratory system; thus, the average values in Table V are preferentially weighted over the large c.m. emission angles. The decrease of the transverse momentum in the extreme c.m. emission angles was noted by Pernegr *et al.*[38]

V. DISCUSSION

1. Observed Features and Theories for Jets

The present experiment has investigated the following features of high-energy jets: (i) composition of produced particles, (ii) the transverse momenta of different secondary particles, and (iii) the c.m. momentum distribution of different particles; these features are found to be dependent on the c.m. emission angle. The index of persistency P is related to (iv) inelasticity of interaction μ as $P=1-\mu$. Besides these, previous extensive investigations of jets have yielded information concerning other features such as (v) variation of multiplicity of the produced shower particles with the energy of the primary and (vi) anisotropic emission of the secondary particles in the c.m. system. So far few attempts have been made to measure (vii) the total and elastic scattering cross sections. Investigations of some features, listed above, suffer from the inaccurate estimate of the primary energy itself.

There have been many theories proposed to explain partially or totally the observed features, listed above, such as those of Heisenberg,[39] LOW,[40] Fermi,[41] Landau,[42] and Bhabha.[43] There also are phenomenological models proposed to explain certain parametric features, such

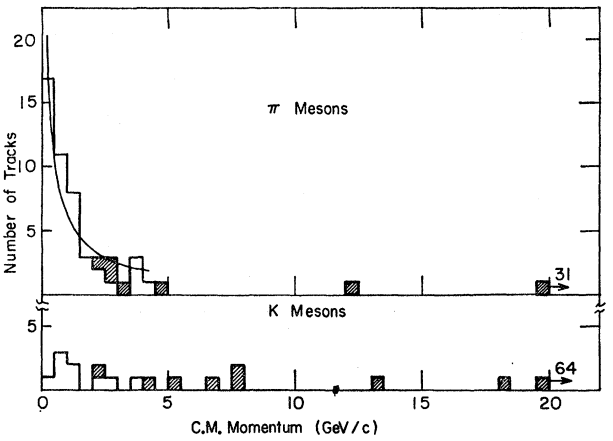

FIG. 8. C.m. momentum distribution for π mesons and K mesons. Shaded regions are the portions of secondaries for c.m. emission angle $\bar{\theta}\geq 175°$. The curve is the best fit for $\bar{\theta}<175°$ in the form $dN\propto\bar{p}^n d\bar{p}$ with $n=-0.8$.

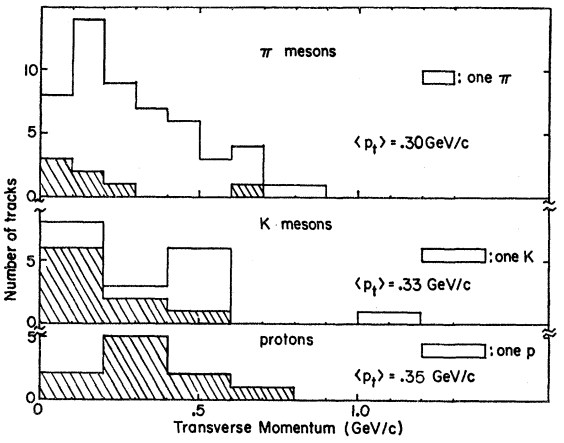

FIG. 9. Transverse momentum distribution for π mesons, K mesons, and protons. Shaded regions are the portions of secondaries for c.m. emission angle $\bar{\theta}\geq 175°$.

[37] J. Nishimura, Soryushiron Kenkyu **12**, 24 (1956); Z. Koba, in *Proceedings of Sixth Annual Rochester Conference on High-Energy Nuclear Physics* (Interscience Publishers, Inc., New York, 1956), p. IV-46; A. Debenedetti, C. M. Garelli, L. Tallone, and M. Vigone, Nuovo Cimento **4**, 1143 (1956); O. Minakawa, Y. Nishimura, M. Tsuzuki, H. Yamanouchi, H. Aizu *et al.*, Nuovo Cimento Suppl. **11**, 125 (1959); M. Schein, D. M. Haskin, E. Lohrmann, and M. Teucher, Phys. Rev. **116**, 1238 (1959); L. F. Hansen and W. B. Fretter, *ibid.* **118**, 812 (1960). See also Ref. 6.

[38] J. Pernegr, V. Šimák, and M. Votruba, Nuovo Cimento **17**, 129 (1960).

[39] W. Heisenberg, Z. Physik. **113**, 61 (1939); **126**, 569 (1949); **133**, 65 (1952).

[40] H. W. Lewis, J. R. Oppenheimer, and S. A. Wouthuysen, Phys. Rev. **73**, 127 (1949).

[41] E. Fermi, Progr. Theoret. Phys. (Kyoto) **5**, 570 (1950); Phys. Rev. **81**, 683 (1951); **92**, 452 (1953); **93**, 1434 (1954).

[42] L. D. Landau, Izv. Akad. Nauk SSSR Ser. Fiz. **17**, 51 (1953).

[43] H. J. Bhabha, Proc. Roy. Soc. (London) **A152**, 559 (1953).

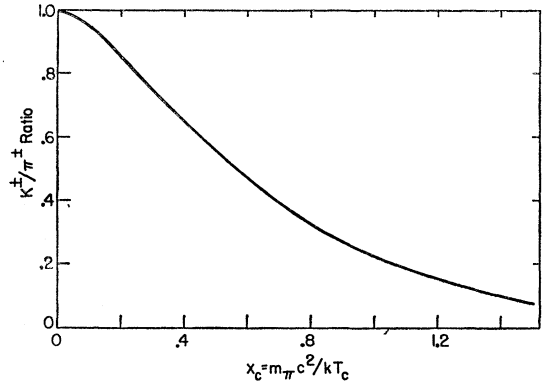

FIG. 10. $K^{\pm}/\pi^{\pm}$ ratio versus critical temperature from the hydrodynamical theory.

as the two-center model,[44] the tunnel model,[45] and the two-fire-ball model.[46] Recently Peters' hypothesis[47] has drawn much attention. Amati *et al.*[48] developed a field-theoretical model for the multiple production of particles.

The three features (i)–(iii) of the present experiment could be studied only for two intervals of c.m. emission angle as tabulated in the Tables III and V; i.e., for $\bar{\theta}\geq 175°$ and $\bar{\theta}<175°$. In the following section, it will be proposed that the hydrodynamical theory[42,49–56] describes the observed features consistently, as far as the K/π ratio, p_t distribution, and $\langle\bar{p}\rangle$ at $\bar{\theta}<175°$ are concerned. In Sec. 3 the Heisenberg theory[39,57] will be discussed for interpretations of the smallness of $\langle p_t\rangle$ and high K/π ratio in the extreme c.m. emission angle $\bar{\theta}\geq 175°$. The Landau theory[42] and Heisenberg theory[39] are two extreme cases of laminar flow and turbulent flow, respectively, in the relativistic hydrodynamical system.[58] So the intermediate theory between the two extreme theories or the application of the two theories to the different c.m. emission angles might be necessary to explain the over-all properties of jets. (See the Sec. 4.)

2. Data for $\bar{\theta}<175°$ in Terms of the Fermi-Landau Theory

The basic assumption of the Fermi-Landau theory was first proposed by Fermi and later modified by Landau. When two very fast nucleons collide, the energy in the c.m. system is released in a very small volume Ω

$$\Omega=\frac{4}{3}\left(\frac{\hbar}{m_\pi c}\right)^3\frac{2m_ic^2}{\bar{E}_0}, \tag{7}$$

where m_i is the nucleon's mass and $\bar{E}_0$ is the total energy of the two colliding nucleons in the c.m. system, and the Lorentz contraction in the direction of the nucleon's motion is taken into account. The nuclear interaction is "strong," the interaction volume Ω is small, and the energy distribution will be determined by statistical laws. Fermi originally took this initial stage of statistical equilibrium as "frozen" and thus the observed final state of multiple production process should reflect the initial equilibrium. Landau modified this view to one in which the observed number of particles in a nuclear interaction does not correspond to the first stage of statistical equilibrium but to the second stage when a *critical* temperature has been reached. Namely, this is the time when, due to the expansion of the system, the mean free path of the created particles becomes comparable with the linear dimension of the system and their mutual interactions decreases sharply. In the process of expansion the system can be visualized as a relativistic hydrodynamical system, since the mean free

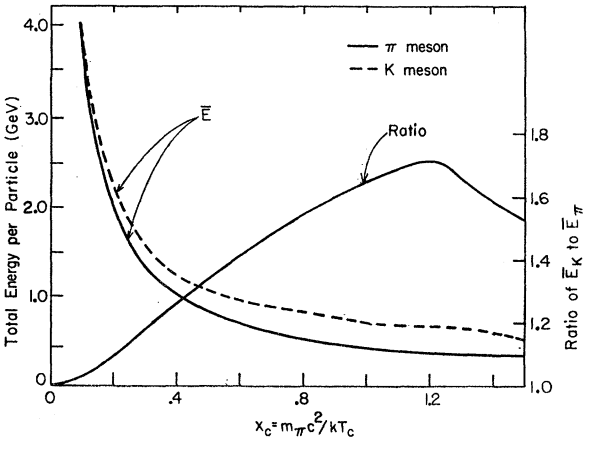

FIG. 11. Average energy $\bar{E}$ of π mesons and K mesons and their ratio in the rest system of the fluid, calculated from the hydrodynamical theory, as a function of the critical temperature.

[44] E. L. Feinberg and D. S. Černavsky, Dokl. Akad. Nauk SSSR **81**, 795 (1951); S. Takagi, Progr. Theor. Phys. (Kyoto) **7**, 123 (1952); W. L. Kraushaar and L. J. Marks, Phys. Rev. **93**, 326 (1954).

[45] F. C. Roesler and C. B. A. McCusker, Nuovo Cimento **10**, 127 (1952); G. Cocconi, Phys. Rev. **93**, 1107 (1954).

[46] K. Niu, Utyusen-Kenkyu **3**, 85 (1958); Nuovo Cimento **10**, 994 (1958); P. Ciok, T. Coghen, J. Gierula, R. Holynski, A. Jurak *et al.*, Nuovo Cimento **8**, 166 (1958); G. Cocconi, Phys. Rev. **111**, 1699 (1958).

[47] B. Peters, Nuovo Cimento **23**, 88 (1963); *Proceedings of the 1962 International Conference on High-Energy Physics at CERN*, edited by J. Prentki (CERN Scientific Information Service, Geneva, 1962), p. 623.

[48] D. Amati, S. Fubini, A. Stanghellini, and M. Tonin, Nuovo Cimento **22**, 569 (1961); **26**, 896 (1962).

[49] S. S. Belen'kij and L. D. Landau, Nuovo Cimento Suppl. **3**, 15 (1956).

[50] Z. Koba, Progr. Theoret. Phys. (Kyoto) **15**, 461 (1956).

[51] S. Amai, H. Fukuda, C. Iso, and M. Sato, Progr. Theoret. Phys. (Kyoto) **17**, 241 (1957).

[52] G. A. Milečin and I. L. Rozental, Nuovo Cimento Suppl. **8**, 770 (1958).

[53] G. A. Milekhin, Zn Eksperim. i Teor. Fiz. **35**, 978, 1185 (1958) [English transls.: Soviet Phys.—JETP **8**, 682, 829 (1959)].

[54] E. L. Feinberg, *Ninth International Annual Conference on High-Energy Physics, Kiev, 1959* (Academy of Sciences, U.S.S.R., 1960), Vol. II, p. 358; Usp. Fiz. Nauk **70**, 333 (1960) [English transl.: Soviet Phys.—Usp. **3**, 159 (1960)].

[55] C. Iso, K. Mori, and M. Namiki, Progr. Theoret. Phys. (Kyoto) **22**, 403 (1959).

[56] D. S. Chernavsky and E. L. Feinberg, *Proceedings of the International Conference on Cosmic Rays at Jaipur, India, 1963* (Tata Institute of Fundamental Research, Colaba, Bombay, India, 1964) Vol. V.

[57] Z. Koba, Progr. Theoret. Phys. (Kyoto) **17**, 288 (1957).

[58] D. Czernawski, Postepy Fiz. **9**, 653 (1958).

path remains small compared with the dimension of the system.

According to the theory, the particle density of the Boson gas ρ at the critical temperature T_c at a certain section of the system is expressed by

$$\rho=\sum_i \rho_i,$$
$$\rho_i=(g_i/2\pi^2)(kT_c/c\hbar)^3F(m_ic^2/kT_c), \quad (8)$$

where

$$F(x_c)=x_c^2\sum_{\nu=0}^{\infty}\frac{K_2[(1+\nu)x_c]}{(1+\nu)},$$
$$x_c=m_ic^2/kT_c,$$

g_i is the statistical weight of the particle of mass m_i, and $K_2(x)$ is a modified Bessel function of the second order.[50,59] The $K^{\pm}/\pi^{\pm}$ ratio as predicted by Eq. (8) as a function of $x_c=m_\pi c^2/kT_c$, is shown in Fig. 10 where $g_{K^\pm}=g_{\pi^\pm}=2$ is assumed. From the present experimental ratio of the number of charged kaons to that of charged pions, 0.34 ± 0.09,

$$kT_c=(1.3\pm0.2)m_\pi c^2. \quad (9)$$

If the K/π ratio for $\bar{\theta}<175°$ is considered ($9/46=0.20\pm0.07$), then

$$kT_c=(0.93_{-0.15}{}^{+0.18})m_\pi c^2. \quad (10)$$

The hydrodynamical theory further predicts the energy density of the produced boson particles at a temperature T as

$$\epsilon_i(T)=(g_ikT/2\pi^2)(kT/c\hbar)^3G(m_ic^2/kT), \quad (11)$$

where

$$G(x)=x^2\sum_{0=\nu}^{\infty}\frac{1}{1+\nu}\left[\frac{3K_2(\langle 1+\nu\rangle x)}{1+\nu}+xK_1(\langle 1+\nu\rangle x)\right],$$
$$x=m_ic^2/kT,$$

and $K_1(x)$ is a modified Bessel function of the first order.[50,59] So the energy per particle at the critical temperature T_c becomes

$$\bar{E}_i=\epsilon_i(T_c)/\rho_i(T_c)$$
$$=kT_cG(m_ic^2/kT_c)/F(m_ic^2/kT_c). \quad (12)$$

A graph of this function at various $x_c=m_\pi c^2/kT_c$ is shown in Fig. 11 for kaons and pions, as calculated from Refs. 50 and 59. Also shown is the ratio of $\bar{E}_K$ to $\bar{E}_\pi$, which stays around unity for $kT_c\gg m_\pi c^2$, and goes up, in a complicated manner, eventually to $3.54=m_K/m_\pi$ in the nonrelativistic limit. The over-all average momenta of kaons and pions ($\langle\bar{p}_K\rangle=8.1$ GeV/c, $\langle\bar{p}_\pi\rangle=2.1$ GeV/c) are rather large when Eq. (12) gives $\bar{E}_K=0.77$ GeV and $\bar{E}_\pi=0.46$ GeV at $kT_c=m_\pi c^2$. This would immediately suggest an explanation in terms of higher critical temperature than $m_\pi c^2$ as seen from Fig. 11. The same situation persists even if only the average momenta of kaons and pions for $\bar{\theta}<175°$ are taken into consideration. While it may not be ignored

[59] S. Z. Belen'kij, Dokl. Akad. Nauk SSSR **99**, 523 (1954).

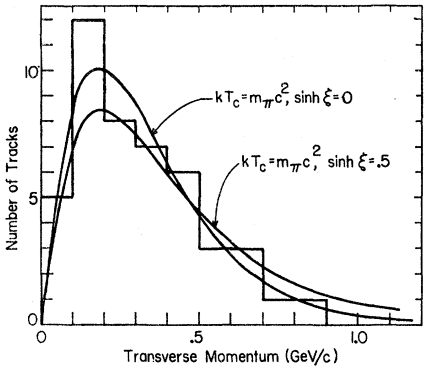

FIG. 12. Transverse momentum distribution of π mesons for $\bar{\theta}<175°$. The theoretical curves are from Milekhin's three-dimensional hydrodynamical theory.

that the possible overestimates of the primary energies, in general, result in overestimates of the c.m. momenta proportionally through the Lorentz factor $\gamma_{\text{Cast}}=(E_{\text{Cast}}/2m_\pi c^2)^{1/2}$, another natural explanation could be given by assuming that a portion of the fluid, that is responsible for the isotropic emission of pions and kaons according to Eq. (12), has a c.m. velocity $\bar{\beta}$. While $kT_c=m_\pi c^2$, the average c.m. momenta of kaons and pions will reach the same magnitude as the present data for $\bar{\theta}<175°$ if $\bar{\beta}=0.88$ ($\bar{\gamma}=2.1$), which should be taken as an upper limit because of frequent overestimate of the Lorentz factor and the strong bias of the present experiment, if $\bar{\beta}$ is indeed different from zero. However, the ratio of the c.m. average momenta of kaons and pions 1.5 ± 0.5, which is far less biased than the individual momenta, is consistent with

$$kT_c=m_\pi c^2, \quad (13)$$

since it can be shown that the ratio of average momenta of kaons and pions is approximately Lorentz invariant provided that $\bar{\beta}>0.3$ and that kaons and pions are emitted isotropically in the fluid.

The transverse momentum distributions are consistent with a critical temperature $kT_c\approx m_\pi c^2$. The over-all distribution of pion transverse momentum shows very good agreement with the calculations (for $kT_c=m_\pi c^2$) of Milečin and Rozental[52] and Milekhin[53] as the experiments of Debenedetti *et al.*[60] and Hansen *et al.*[61] previously showed. The transverse momentum distribution of pions for $\bar{\theta}<175°$ is shown in Fig. 12, together with the theoretical calculations by Milekhin[53] for the two parameters $kT_c=m_\pi c^2$ and $\sinh\xi=0$ and 0.5, where ξ is defined as the hydrodynamical transverse velocity at the moment of breakup. The best fit is obtained when

$$kT_c=m_\pi c^2 \quad \text{and} \quad \sinh\xi=0, \quad (14)$$

which means that the transverse velocity at the moment of breakup is negligible. Thus, the one-dimensional hydrodynamical theory gives an over-all satisfactory fit to the data for this angular interval. Here it must be

[60] See A. Debenedetti *et al.*, Ref. 37.
[61] See L. F. Hansen *et al.*, Ref. 37.

noted that Eq. (6) is also consistent with $n=-1$, which is predicted by the hydrodynamical theory.

3. Data for $\bar{\theta}\geq 175°$ and the Interpretation

Several disagreements emerge when the K/π ratio, the average momenta of pions and kaons, and the transverse momenta for $\bar{\theta}\geq 175°$ are studied under the light of the hydrodynamical theory. The large K/π ratio and $\langle\bar{p}\rangle$ suggest a large critical temperature of the fluid (Fig. 10)

$$kT_c \gg m_\pi c^2 \tag{15}$$

while the small transverse momenta observed in this angular region can only be explained in terms of the critical temperature $kT_c \ll m_\pi c^2$. The average c.m. momenta are affected too much by several high-energy mesons, and the ratio of the c.m. momenta of kaons and pions will not help to clarify the situation.

The smallness of the transverse momenta in the region of extreme backward emission is suggestive of the Heisenberg theory since this theory predicts

$$p_t \approx m_\pi c. \tag{16}$$

Moreover, according to Ref. 50, the critical temperature in the Landau theory is determined mainly by the pion-pion interaction and is common to all the elements of the expanding hydrodynamical system, so that one can expect the *same* composition of particles in *all* directions in the c.m. system. But, in the Heisenberg theory, the transverse energy is so low that few heavy mesons can appear in the perpendicular direction in the c.m. system.[57] So the high concentration of heavy particles in the extreme backward emission angle which is observed in the present experiment supports the prediction of the Heisenberg theory. The early indication of this trend is already mentioned in Ref. 6. The over-all ratio of kaon production to pion (0.34 ± 0.09) is consistent with what the Heisenberg theory predicts; i.e., 0.29, taken from Table 3.1 of Ref. 57 for $E_0/M=10^3$. The large c.m. momenta may be attributed to the high velocity of the disturbance wave. But this theory can not explain the large transverse momenta for $\bar{\theta}<175°$. The internal consistency of the interpretation in the previous section might favor definitely the hydrodynamical theory for the data for $\bar{\theta}<175°$.

4. Correlation Between the Different Interpretations

Milekhin[62] clarified the interrelation between the Landau and Heisenberg theories through the generalized equation of state in the hydrodynamical theory. Originally Landau assumed, as an additional postulate to his theory, the equation of state

$$p=c_0^2\epsilon, \tag{17}$$

where p is the pressure, ϵ the energy density, and c_0^2 the square of the sound velocity of the medium in units of the velocity of light:

$$c_0^2=\tfrac{1}{3} \tag{18}$$

from an analogy with the black-body radiation. But it turned out that when

$$c_0^2=0 \tag{19}$$

the hydrodynamical description becomes equivalent to the Heisenberg theory. Since the data for $\bar{\theta}\geq 175°$ in the present experiment favor an interpretation in terms of the Heisenberg theory and those for $\bar{\theta}<175°$ in terms of Landau theory, then it might be concluded that c_0^2 either varies according to the c.m. emission angle or is some number between 0 and $\frac{1}{3}$. But it seems clear that the two views are sufficient to describe the parametric features observed in the present experiment.

VI. CONCLUSIONS

The present experiment has made full use of the large dimension of the stack, which was found to be extremely valuable both in the tracing of tracks and in the observation of the gradual change of ionization as the secondaries traversed the block of emulsion. Moreover, the local normalization of the grain density to that of high-energy electrons and the good statistics of grain counts contributed to improve the method of identity assignment. The present experiment shows good agreement with the theory of ionization loss in the transminimum region to an extent which enabled discrimination of kaons from pions up to $p\beta$ of ~ 10 GeV/c.

Among 82 secondaries analyzed, the composition found consisted of 53 pions, 18 kaons, 10 protons, and one hyperon. The average c.m. momenta were 2.1 and 8.1 GeV/c for pions and kaons, respectively, in the solid angle analyzed; the transverse momenta were 0.30, 0.33, and 0.35 GeV/c, respectively, for pions, kaons, and protons. The over-all results of the present experiment may be roughly accounted for by the hydrodynamical theory with a critical temperature $kT_c=m_\pi c^2$, consistent with the observed average K/π ratio and the transverse momenta.

The baryons carried, on the average, a fraction 0.5 ± 0.2 of the available energy per nucleon in the c.m. system of the collision. This method, if refined further with better statistics, is a good means of measurement of the inelasticity of nuclear interaction of high-energy jets since it is not affected by the inaccuracy of the primary energy estimate to a good approximation. From analysis of the four-momentum transfer of the 11 baryons by assuming that the identified baryons are surviving target nucleons, it has been inferred that $(-\Delta^2)^{1/2}=1.1$ GeV.[63] This fact may coincide with the

[62] G. A. Milekhin, in *Proceedings of 1959 International Conference on High-Energy Physics, at CERN* (CERN, Geneva, 1959), Vol. II, p. 397.

[63] R. W. Huggett, K. Mori, C. O. Kim, and R. Levi Setti, *Proceedings of the International Conference on Cosmic Rays at Jaipur, India, 1963* (Tata Institute of Fundamental Research, Colaba, Bombay, India, 1964), Vol. V.

central character of the inelastic nuclear process, deduced from the present experiment. Recent observations of the large-angle p-p scatterings at accelerator energies were explained in terms of the statistical theory, which supports our view.[64]

Even if the number of tracks analyzed is small, the qualitative structure in the c.m. emission angles is conspicuous. The observed features in the extreme backward region of c.m. emission angles are as follows: (i) There are more heavy particles than in the perpendicular region in the c.m. system; (ii) the average c.m. momenta become very large; (iii) the transverse momenta become small. The increase of transverse momentum with the mass of the secondary particle is noticeable.

For the observed features in $\bar{\theta}<175°$, the hydrodynamical theory with $kT_c \cong m_\pi c^2$ gives a consistent description except for the fact that an average c.m. velocity of the fluid that is responsible for the isotropic emission of mesons must be assumed to get the magnitude of the average c.m. momenta observed. The fact that the c.m.-momentum distribution of pions is of the form $dN \propto \bar{p}^n d\bar{p}$ with $n=-0.8\pm0.4$ supports this view. But for $\bar{\theta}\geq 175°$ an interpretation in terms of the Heisenberg theory is favored.

The existence of several very high-energy secondary mesons in the extreme c.m. emission angles, which may coincide with the observation of production of the very high-energy gamma ray in a jet,[12] must be examined with better statistics. These mesons may be the decay products of "persistent" excited nucleon states. Or phenomenologically, they may have the function of the energy carrier, which is built in the hydrodynamical theory to carry away about half of the available energy in the c.m. system.[51]

The theoretical correlation between the two extreme views was discussed by Milekhin.[62] The consequence of the present view that both the Landau and Heisenberg theories might contribute may yield a variation of the multiplicity of shower particles n_s as a function of the primary energy E_0 of the form

$$n_s = aE_0^{1/4} + bE_0^{1/2},$$

where a and b are constants. The total cross section of interaction would increase slightly by consequence of the contribution of the Heisenberg disturbance wave. The ratio of kaon production to that of pions would not vary very much from the known rate of production at accelerator energies.

ACKNOWLEDGMENTS

The author wishes to express his hearty gratitude to his thesis adviser Professor R. Levi Setti whose guidance has been invaluable throughout the course of the present work. He is also much indebted to Professor M. Koshiba of the University of Tokyo who originally recommended the present project and gave generous help during the initial phase of the work. He is grateful to Dr. C. H. Tsao for helpful discussions and check of numerical calculations through the computer. Thanks are due to Dr. J. Kidd and Dr. K. Rybicki for helpful criticisms and valuable discussions. Discussions with Professor Y. Nambu, Dr. K. Mori, and Professor J. Gierula were deeply appreciated by the author. Mrs. J. Para was very helpful in the tracing. D. Spector was appreciated for calculations of the mass spectrum through IBM 7094. The author is very grateful to Miss B. Gygi, L. Henry, P. Li, Mrs. I. Orr, G. Schultz, and P. Waltz for their assistance in tracing and analysis. Our thanks are also due to Dr. J. Hornbostel of the Brookhaven National Laboratory for the loan of a Koristka digitized scattering microscope.

APPENDIX

1. Grain Density Measurements

Grain counting was performed with 53× objective and 12.5× ocular. As discussed in Sec. III, the convention for counting is very critically relevant to the ratio of the plateau to the minimum, which, in turn, sets the delta-ray energy limit T_0. In the convention adopted here, those grains which were not strictly aligned with the particle path were rejected in counting, but even small grains were counted if they aligned well. Repeated observations of grain counts over the same track by the same observer showed consistently the same value within 0.2% over a substantial lapse of time. The grain density was not measured within 1 cm from the plate edges. Unfortunately, the grain density varied from one plate to another and had a dependence on the depth of emulsion. The grain density of a secondary g was normalized to the average grain density of high-energy electrons g_0. This procedure was carried out effectively by counting the grains through a whole plate from the glass bottom to the air surface of the emulsion, both for the secondary and for the high-energy electron tracks. This normalized grain density, $g^*=g/g_0$, was obtained by individual observers to eliminate subjective factors in the counting procedure. The grain density of flat secondaries was normalized to that of the high-energy electrons at the same depth of the emulsion in the vicinity of the secondary, after constructing a curve similar to that shown in Fig. 1. The electron tracks were carefully selected and low-energy tracks were discarded. The radiative correction[65] was inferred as negligible from the measurements of the normalized grain density of the highest energy electrons in the cores of jets ($\gamma\geq 4\times10^3$), $g^*=0.99\pm0.03$, where the normalizing

[64] L. W. Jones, Phys. Letters **8**, 287 (1964); R. Hagedorn (private communication); G. Cocconi, Nuovo Cimento **33**, 643 (1964).

[65] K. I. Alekseyeva, G. B. Zhdanov, E. A. Zamchalova, M. Novak, M. I. Tretyakova, and M. N. Shcherbakova, in Proceedings of the 3rd International Conference on Nuclear Photography, Moscow, 1962, p. 396 (unpublished); G. B. Zhdanov, M. I. Tret'yakova, V. N. Tsytovich, and M. N. Shcherbakova, Zh. Eksperim. i Teor. Fiz. **43**, 342 (1962) [English transl.: Soviet Phys.—JETP **16**, 245 (1963)].

procedure was the same as for the secondaries by using the shower electrons ($\gamma \simeq 200$). The average grain density of shower electrons g_0 from different showers in a given plate showed consistently the same value. The values of g^* for the same track for several successive plates usually showed good regularity. Errors on g^*, Δg^*, were taken as

$$\Delta g^* = (1/N_g + 1/N_{g0})^{1/2},$$

where N_g and N_{g0} are the numbers of grains counted, respectively, for the secondary and high-energy electron tracks.

2. Scattering Measurements

The multiple scattering measurements were made on Koristka R-4 and MS-2 microscopes with 100× and 90× objectives with a total magnifying power of about 1200×; the microscope lamp was always turned on 2 h before measurement. Scattering measurements were not performed if the secondary was within about 4 cm from the plate edges. The standard sagitta method[21,22] was used to obtain $p\beta$. For the present experiment the value of the scattering constant K was taken to be 26.7, 27.6, 28.5, and 29.3, respectively, for 250-, 500-, 1000-, and 2000-micron cells.[66] This value K refers to $\beta=1$ with the cutoff procedure, which means that second differences that exceed four times the average are eliminated in the next average-taking procedure. In practice, the measured average second differences, $\langle D_2(1)\rangle_{\text{meas}}$, contain contributions from effects other than multiple Coulomb scattering. Among these effects[67] the combined effects of stage noise and reading noise were estimated from measurements of second differences on a Bausch and Lomb straight line. The combination of spurious scattering with the stage noise, reading noise, and grain noise were estimated from scattering measurements on flat primary tracks of high energy. Results of these measurements are tabulated in Table VI. As seen in this table, while the stage noise is almost independent of the cell size, other listed noises are probably due to small gradual distortions of the plates in packing and due to the differential shrinkage of emulsion during processing. Some effect might come from the fact that the average second differences listed for larger cell lengths resulted from taking completely overlapping second differences from the measurements for the basic cell length rather than taking the direct measurements for the actual cell lengths.

TABLE VI. The noise level by second differences in microns.

Cell length t	By primaries	By straight line in MS-2
250 microns	0.107±0.003[a]	
500	0.112±0.008 (0.124)[b]	(0.059±0.008)
1000	0.165±0.017 (0.160)	(0.078±0.014)
2000	0.298±0.079 (0.240)	(0.086±0.022)

[a] Errors quoted are only statistical.
[b] The numbers in the brackets are for MS-2.

The noise elimination was carried out on the assumption that the noise contribution δ is independent of cell length as follows:

$$\langle D_2(1)\rangle^2_{\text{meas}} = \delta^2 + \left(\frac{K(1)t_1^{3/2}}{573p\beta}\right)^2, \tag{20}$$

where $\langle D_2(1)\rangle_{\text{meas}}$ is the average second difference of the basic cell length t_1,

$$\langle D_2(n)\rangle^2_{\text{meas}} = \delta^2 + \frac{K^2(n)n^3}{K^2(1)}\left(\frac{K(1)t_1^{3/2}}{573p\beta}\right)^2, \tag{21}$$

where $\langle D_2(n)\rangle_{\text{meas}}$ is the average second difference by the completely overlapping procedure of the cell length nt_1. Then from Eqs. (20) and (21)

$$\langle D_2(1)\rangle = \frac{K(1)t_1^{3/2}}{573p\beta} = \frac{[\langle D_2(n)\rangle^2_{\text{meas}} - \langle D_2(1)\rangle^2_{\text{meas}}]^{1/2}}{[[K(n)/K(1)]^2 n^3 - 1]^{1/2}}. \tag{22}$$

The basic cell length used was 250 microns or 500 microns in this experiment. The errors of the final values were processed according to Di Corato *et al.*[68] whose methods were based on the theory of D'Espagnat.[69] In most of the cases the actual error was either $1.46/\sqrt{n_D}$ for $n=2$ or $1.92/\sqrt{n_D}$ for $n=4$, where n_D is the number of second differences of the basic cell length. For each secondary, the two sets of values of $p\beta$ and its error were processed by a combination of $\langle D_2(2)\rangle_{\text{meas}}$ and $\langle D_2(1)\rangle_{\text{meas}}$ or by that of $\langle D_2(4)\rangle_{\text{meas}}$ and $\langle D_2(1)\rangle_{\text{meas}}$ through Eq. (22), and they were examined for consistency of measurements. In a few cases, when the two values of $p\beta$ of the same secondary, which were obtained as described above, were not in agreement within their errors, then the value of $p\beta$ and its error, which were obtained through the combination of $n=4$ and $n=1$ values, were adopted. The third differences were processed in a similar way to get $p\beta$.[68] The average ratio of $p\beta$ deduced from the third differences and that from the secondary differences on the same track was 0.99, which shows that, on the average, there are not serious distortions in the stack. All these values of $p\beta$ were also tested for consistency with those that were obtained independently by eliminating the total noise assuming the noise of the corresponding cell length listed in Table VI.

[66] C. Fichtel and M. W. Friedlander, Nuovo Cimento **10**, 1032 (1958).
[67] R. Levi Setti, Nuovo Cimento 8, 96 (1951).
[68] M. Di Corato, B. Locatelli, and D. Hirschberg, Nuovo Cimento Suppl. 4, 448 (1956).
[69] B. D'Espagnat, Compt. Rend. 232, 800 (1951).